Clinical Cancer Investigation Journal-ISSN: 2278-0513

Modeling of an Autothermal Catalytic Monolith Reformer to Obtain Hydrogen for Fuel Cells (Considering Inlet Oxygen Effect)

Abstract

Due to the increasing use of fuel cells in different industries and as an on-site application, there is a need to develop on-site centers for hydrogen production. In the present paper, a catalytic monolithic reformer including the methane autothermal reforming process was 3D modeled. The catalyst used in the present modeling was 5% $Ru - \gamma\ Al_2O_3$. This modeling was based on the simultaneous solution of the conservation equations, in which the effect of performed reactions was also considered. One channel of this monolithic reactor was used as the computational domain. The results of this modeling were in good agreement with the laboratory data available in the literature. This model was used to estimate the performance of the reformer in other operating conditions. The parameter studied in the present research was the inlet oxygen/methane molar ratio. Finally, it was found that to achieve the maximum hydrogen content in the range of operating parameters, the molar ratios of reactor inlet oxygen/methane and steam/methane should be equal to 0.445 and 3.8, respectively.

Keywords: *Hydrogen, Autothermal Reforming, Methane, Monolithic Reactor*

Farnaz Mahdavi Dehkharghani

Ph.D., Department of Energy and Environment, Shahid Beheshti University, Tehran, Iran.

Farnazmahdavi841@gmail.com

Introduction

A Fuel cell directly converts the chemical energy of a fuel into electrical energy. The fuel cell is one of the new technologies for energy production in the future because of its high power density, production of environmentally friendly by-products, and fast recharging. It is also an acceptable variety for energy production with standard methods. The most vital advantage of the fuel cell compared to reciprocating and Stirling engines is the possibility of achieving higher potency in converting fuel into electricity. This feature is very appropriate in contaminated areas. Hydrogen is the preferred fuel for fuel cells. Hence, the employment of fuel process systems to provide the hydrogen required for fuel cells on-site is recommended. The employment of these fuel process systems provides the possibility of mixing the high energy density of fuels and the high power density of the fuel cell and creates a system with high efficiency. So far, a lot of research has been done to investigate fuel processing systems in the form of laboratory work and modeling. Veser et al. **[1]** modeled the catalytic oxidation of methane on a Pt catalyst in a monolithic reactor in a one-dimensional manner. Their model only included mass and energy balances for the gas phase and monolithic catalyst. In their study, they considered only the reaction that happened on the surface of the catalyst. Canu et al. **[2]** modeled the catalytic combustion of methane on Pt in a monolithic reactor using Computational Fluid Dynamics (CFD) analysis. The balance equations of mass, energy, and momentum in this research were solved work using CFX software. In their study, it was found that the gas phase reaction has little impact on methane conversion percentage. Ghadrdan et al. **[3]** studied a 2D model for the catalytic combustion of methane in a monolithic reactor channel. They did not compare their modeling with the experimental model and only investigated the effect of various parameters such as inlet gas temperature, rate, and concentration on the Nusselt number. However, the authors emphasized that their results are theoretically correct. Stutz et al. **[4]** solved the mass, energy, and momentum balance equations for fluid flow in a channel of a monolithic reactor and assumed an adiabatic wall. To model the chemical reaction, they considered 38 surface reactions considering 7 gaseous species and 12 species adsorbed on the surface. Chaniotis et al. **[5]** used the partial oxidation reaction of methane to produce hydrogen in the channel of a monolithic reactor. They considered a channel with a diameter of 1 mm and a length of 10 mm. In their studies, they concluded that hydrogen production is strongly dependent on the equivalent ratio. In the range of equivalent ratio between 0.6 and 1, the amount of hydrogen produced was high and the hydrogen yield was about 70-80%. Shi et al. **[6]** studied isooctane steam reforming on Rh catalyst in a monolithic reactor using 3D CFD modeling. They assumed the performance of all channels in the studied monolithic reactor is the same so chose only one channel of the reactor as their computational domain. Di Benedetto et al. **[7]** modeled the thermal behavior of a monolithic microreactor (especially a microreactor with three and five channels). They concluded that the behavior of a multi-channel structure cannot be extrapolated from the behavior of a single-channel structure due to the heat losses, and it is necessary to model the entire monolithic microreactor. However, the time required to model a three- or five-channels reactor is about three and five times the required time to model a single-channel reactor, respectively. Deutschmann et al. **[8]** modeled the 2D partial oxidation of methane on an Rh catalyst inside a channel of a

monolithic reactor. They concluded that the percentage of methane conversion and selectivity of synthesis gas increases with increasing temperature. Also, increasing the reactor pressure reduces the methane conversion percentage, while the selectivity of the synthesis gas decreases only slightly. Ding et al. **[9]** modeled the partial combustion of methane on an Rh-coated monolith using CFD modeling. In this 2D modeling, the effects of conductive heat transfer from the wall, channel diameter, and specific catalytic surface on reactor performance were considered. They reported that at a constant specific surface of the catalyst, the maximum wall temperature decreases with increasing channel diameter. Mei et al. **[10]** selected a cylindrical metal monolithic reactor for methane autothermal reforming. In this model, the effects of the feed rate ratio of two sections, inlet temperature, feed concentration, and reactor structure were investigated, however, parameters were not optimized in this study. To achieve the required thermal power of the reforming process, a higher rate of reforming to combustion, a higher inlet temperature, and a suitable arrangement of catalyst distribution have been suggested. Shi et al. **[11]** developed a numerical model to investigate the performance of a monolithic catalytic reformer in which normal autothermal reforming of hexadecane ($C_{16}H_{34}$) has occurred. In their study, they investigated the effect of the thermal conductivity of the solid material that the reactor was made of. They concluded that the thermal conductivity of the reactor material affects the temperature profile inside the reactor, while its effect on the molar percentage of H_2, CO, and CO_2 was negligible. Liu et al. **[12]** designed a monolithic reactor in which the mass transfer rate was higher. To achieve better mass transfer, a porous material with high thermal conductivity was placed on the inner wall of the monolithic base. Steam reforming is endothermic while partial oxidation is exothermic. Reactants for autothermal reforming include steam, oxygen, and fuel. Autothermal reforming is a combination of steam reforming and partial oxidation. The most important goal of this research is to numerically investigate the methane autothermal reforming process using 3D modeling. With the help of modeling results, changes in temperature and concentration of components can be checked at any point inside the reactor. Therefore, the present research aims to model the autothermal monolithic catalytic reformer for hydrogen production for fuel cells considering the effect of inlet oxygen.

Characteristics of modeled monolithic reactor

Rabe et al. **[13]** used a monolithic reactor equipped with a thermocouple (TC) to record the temperature throughout the reactor. There was a plate for better mixing of gases in the initial zone of this reactor and before the first monolithic zone. This plate provided a laminar flow to pass through the monolithic zone. Also, there were three monolithic zones, in which only one zone used a catalyst, and the other two were without a catalyst. The catalyst used in the present laboratory work was 5% $Ru-\gamma\,Al_2O_3$. They also studied the effect of two catalytic monolith zones and concluded that the presence of a second catalytic zone has no significant effect on the reactor performance. The diameter and length of each monolithic zone were 3.5 cm. The number of channels of a monolithic reactor is usually defined as the number of cells per square inch (cpsi), which was 400 cpsi for the used reactor, and there were about 597 channels considering the diameter of the monolith reactor. Water was pumped into an evaporator, mixing the steam with methane. The steam/methane mixture was preheated to 275 °C, and oxygen entered the reactor at room temperature. To start the test, the reactor was heated up to the catalytic combustion temperature of the inlet feed (about 500 °C) by a heater, and external heating of the reactor was stopped after the combustion reaction. Figure 1 shows a view of this reactor.

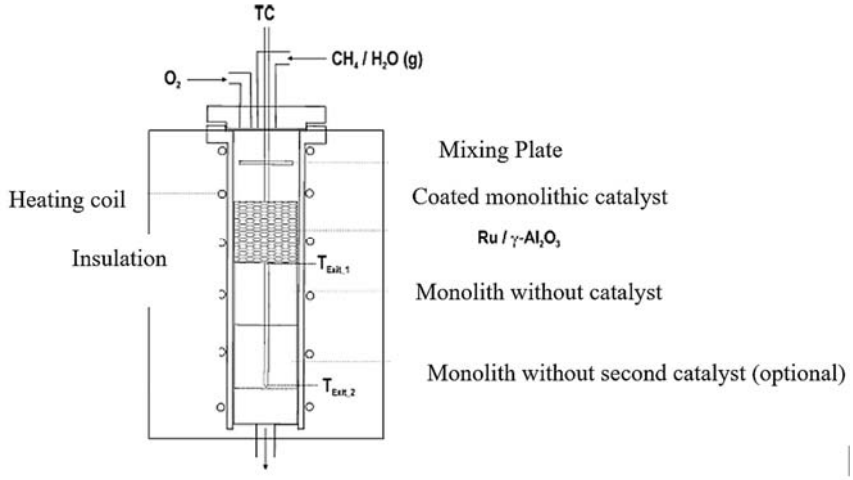

Fig. 1. The reactor used by Rabe **[13]**

Modeling the entire reactor is very expensive and time-consuming. Thus, it is assumed that the behavior of all channels is the same and similar to the behavior of the entire reactor, so only one channel of this reactor was modeled. The channels of this monolithic reactor were considered cylindrical; therefore, the symmetry of this type of channel was beneficial, and only one-quarter of the channel was needed to model. The diameter of each monolithic channel used by Rabe **[13]** was 0.9 mm, and its length was 3.5 cm for each monolithic zone. The initial mixing zone was omitted to model this set, and it was assumed that the gas mixture entering the first monolithic zone was completely homogeneous. According to the assumption, only three monolithic zones were considered in the modeling, equivalent to a length of 10.5 cm. Since the length/diameter ratio of the channel was much higher, only a part of the meshed surface of the used geometry is given in Fig. (2).

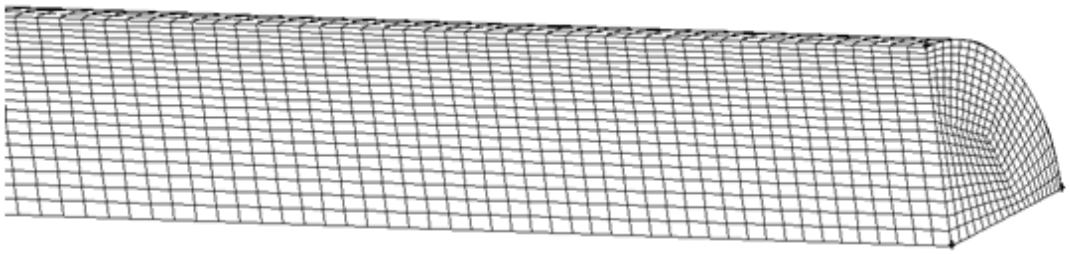

Fig. 2. The meshed surface of the geometry used in modeling

There were about 37500 meshes on the volume. Since the temperature and species concentration changes at the reactor inlet are fast, the number of meshes considered at the beginning of the reactor was more.

Assumptions and equations used in modeling

According to the laboratory results of Rabe et al. **[13],** when the Weight Hourly Space Velocity (WHSV) (the ratio of the reactant mass fed to the reactor per hour to the catalyst mass, 3.1 g 5% Ru-γAl_2O_3 per monolith) is equal to 119 hr^{-1}, the R_e number in the channel of the used monolithic reactor will be equal to 32, indicating that the flow in the channel is laminar. The fluid flow inside the channel and the gas mixture were assumed incompressible and ideal, respectively. Since the operating pressure inside the reactor was 2/1 bar and the pressure drop in the monolithic reactor was very small, these assumptions were reasonable. The modeling of this system was performed in a steady state. The equations of continuity, momentum, energy, and chemical species considered were as follows **[14].** In the following, the methods of calculating the parameters of these equations are presented, adapted from the literature **[14].** These equations were solved using FLUENT 6.3.26 software.

$$\frac{\partial \mathrm{uj}}{\partial \mathrm{x_j}} = 0 \quad (1)$$

$$\rho . u_j \frac{\partial u_i}{\partial x_j} = -\frac{\partial p}{\partial x_i} + \frac{\partial \tau_{ij}}{\partial x_j} + \rho g_i \quad (2)$$

$$\rho . u_j \frac{\partial h}{\partial x_j} = \frac{\partial}{\partial x_j}\left(k_{eff} \frac{\partial T}{\partial x_j} - \sum_{i=1}^{N} h_i J_{ij}\right) + u_j \frac{\partial p}{\partial x_j} + S_h \quad (3)$$

$$\rho . u_j \frac{\partial Y}{\partial x_j} = -\frac{\partial J_{ij}}{\partial x_j} + R_i \quad (4)$$

Where u (m/s) is gas velocity, ρ (kg/m^3), gas density, p (Pa), static pressure, τ_{ij} (Pa), laminar flow stress tensor, ρg (N/m^3), gravitational body force per unit volume, h (kJ/kg), enthalpy, K_{eff} (W/m.K), the effective thermal conductivity (ETC), T (K), the temperature of the gas mixture, h_i (kJ/kg), the enthalpy of specie i, and J_{ij} (kg/m^2s), the diffusive flux of specie i in the j-direction, which is assumed to include the full multicomponent diffusion and heat-induced diffusion. N is the total number of gas species, S_h, is the energy source resulting from the chemical reaction (kW/m^3), Y_i, the local mass percent combination of the species, and R_i (kg/m^3.s), is the net production rate of specie i by chemical reaction. The stress tensor of laminar flow (τ_{ij}) is obtained from the following equation:

$$\tau_{ij} = \mu(\frac{\partial u_i}{\partial x_j} + \frac{\partial u_j}{\partial x_i} - \frac{2}{3}\frac{\partial u_1}{\partial x_1}\delta_{ij})$$

(5)

Where μ (N.s/m^2) is viscosity. The first two terms on the right of the energy equation (Eq. 3) are the energy transferred due to thermal conduction and species diffusion. The thermal energy produced by the viscous shear effect in the flow is neglected. The effective thermal conductivity for the fluid flow in a channel is similar to fluid thermal conductivity, and for the fluid flow in a porous medium is obtained from the following equation:

$$Keff = \varepsilon K_f + (1-\varepsilon)K_s$$

(6)

Where ε is the substrate porosity coefficient, K_f, is the thermal conductivity of the fluid, and K_s is the thermal conductivity of the solid material. Enthalpy, h (kJ/kg), for an ideal gas mixture, is defined as follows:

$$h = \sum_i^N Y_i h_i$$

(7)

Furthermore, h_i is obtained as follows:

$$h_i = \int_{T_{ref}}^{T} C_{p,i}\,dT$$

(8)

Where $C_{p,i}$ (kJ/kg.K) is the specific heat of the specie, i and T_{ref} are the reference temperature (T_{ref} in the present research was 298.15 K). The term of the energy source, S_h (kW/m^3), is calculated from the following equation:

$$S_h = -\sum_i \frac{h_i^\circ}{M_{w,i}} R_i$$

(9)

Where h_i° (kJ/mol) is the formation enthalpy of specie i and $M_{w,i}$ (kg/mol) is the molecular weight of specie i. Since the molecular diffusion process is important in the fuel reformer, the diffusive flux of specie i, J_{ij}, is calculated using the full multicomponent diffusion method based on the Maxwell-Stefan equation:

$$J_{ij} = -\sum_{k=1,\neq i}^{N} \rho D_{ik}\frac{\partial Y_k}{\partial x_j} - D_{T,i}\frac{1}{T}\frac{\partial T}{\partial x_j}$$

(10)

Where $D_{T,i}$ is the thermal diffusion coefficient for specie i in the mixture and $D_{i,k}$ is defined as follows:

$$D_{i,k} = [D] = [A]^{-1}[B]$$

(11)

$$A_{ii} = -(\frac{X_i}{d_{iN}}\frac{M_w}{M_{w,N}} + \sum_{k=1,\neq i}^{N}\frac{X_k}{d_{ik}}\frac{M_w}{M_{w,i}})$$

(12)

$$A_{ik} = X_i(\frac{1}{d_{ik}}\frac{M_w}{M_{w,k}} - \frac{1}{d_{iN}}\frac{M_w}{M_{w,N}})$$

(13)

$$B_{ii} = -(X_i\frac{M_w}{M_{w,N}} + (1-X_i)\frac{M_w}{M_{w,i}})$$

(14)

$$B_{ik} = X_i(\frac{M_w}{M_{w,k}} - \frac{M_w}{M_{w,N}})$$

(15)

Where [A], [B], and [D] are matrices with a size of (N-1)×(N-1). X_i is the mole fraction of specie i, M_w, the molecular weight of the mixture, $M_{w,N}$, the molecular weight of specie N, and $d_{i,k,}$ the binary mass diffusion coefficient for specie i in specie k. The thermal diffusion coefficient is calculated from the following equation:

$$D_{T,i} = -2.59\times10^{-7}\,T^{0.659}\,[\frac{M_{w,i}^{0.511}X_i}{\sum_{i=1}^{N}M_{w,i}^{0.511}X_i} - Y_i][\frac{\sum_{i=1}^{N}M_{w,i}^{0.511}X_i}{\sum_{i=1}^{N}M_{w,i}^{0.489}X_i}]$$

(16)

The binary mass diffusion coefficient is calculated using the Chapman-Enskog equation. This relationship is as follows:

$$d_{ik} = 0.00188\frac{[T^3(\frac{1}{M_{w,i}} + \frac{1}{M_{w,k}})]^{0.5}}{p_{abs}.\sigma_{ik}^2\Omega_D}$$

(17)

Where P_{abs} is the absolute pressure, the Lennard-Jones (LJ) effective diameter for impact Ω_D is diffusion collision integral. σ_{ik} is calculated as follows for a binary mixture:

$$\sigma_{ik} = 0.5(\sigma_i + \sigma_k)$$

(18)

Ω_D is obtained from the following equation:

$$\Omega_D = f(T_D^*) = f(\frac{T}{(\varepsilon/k_B)_{ik}})$$

(19)

Where $(\varepsilon/k_B)_{ik}$ is calculated for the mixture from the following equation:

$$(\varepsilon/k_B)_{ik} = \sqrt{(\varepsilon/k_B)_i.(\varepsilon/k_B)_k}$$

(20)

Where k_B is the Boltzmann constant.
The density of the gas mixture follows the ideal gas law, which is given below:

$$\rho = \frac{P_{op} M_w}{RT}$$

(21)

Where P_{op} (Pa) is the operating pressure.
It is assumed that the thermal conductivity and specific heat of any chemical specie i is a function of temperature, and this temperature equation is a polynomial:

$$\Phi_i = \sum_{k=1}^{m} C_k \, T^{\,k-1}$$

(22)

Where Φ_i thermal conductivity can be assumed or specific heat. The unit of temperature in this relation is (K). The thermal conductivity and specific heat of the gas mixture are calculated from the following equation:

$$\Phi = \sum_{i=1}^{N} Y_i \, \Phi_i$$

(23)

Modeling the reaction mechanism

Since solid and site species are usually very small, they are not considered in modeling the reaction mechanism. The r-th reaction on the wall, which includes only gaseous species, can be written as follows:

$$\sum_{i=1}^{N} g'_{i,r} G_i \leftrightarrow \sum_{i=1}^{N} g''_{i,r} G_i$$

(24)

Where G_i represents the gaseous specie, $g'_{i,r}$, the stoichiometric coefficient for any reactant specie i, and $g''_{i,r}$, the stoichiometric coefficient for any product specie i. The reaction mechanism includes a set of reactions that the above equation applies to all these reactions in the system. The coefficient of species that do not participate in the reaction equals zero. The net rate of production and consumption rate of any specie i, R_i (kmol/m^2.s), is obtained from the following equation:

$$\hat{R}_i = \sum_{k=1}^{N_{rxn}} (g''_{i,r} - g'_{i,r}) r_k \qquad i = 1,2,3,\ldots, N$$

(25)

Where N_{rxn} is the total number of reactions and r_k is the rate of the k-th reaction. Since the effect of gas phase reactions on the overall rate of reactions can be ignored, gas phase reactions are ignored in this modeling, and these reactions are considered only on the catalytic surface of the wall.

Kinetically relationships for methane autothermal reforming using Ru catalyst

For methane autothermal reforming, 6 chemical species, including CH_4, H_2O, O_2, H_2, CO, and CO_2, were considered in the modeling. The stoichiometry of the chemical reactions considered for methane autothermal reforming is equations (9)-(12). Since the amount of CO_2 is more than the amount of CO at the reactor outlet, to better estimate the amount of CO_2 at the reactor outlet, the autothermal reforming process was considered as a combination of the steam reforming process and complete combustion in this modeling. The rate equations provided by Xu and Froment **[15]** were used for the steam methane reforming process and the water-gas shift reaction, and the rate equations given by Ma **[16]** were used for the complete combustion of methane.

$$r_1 = \frac{k_1}{(1 + K^1_{CH_4} p_{CH_4} + K^1_{O_2} \sqrt{p_{O_2}})^2} p_{CH_4} \sqrt{p_{O_2}}$$

(26)

$$r_2 = \frac{k_2}{p^{2.5}_{H_2}} \left(p_{CH_4} p_{H_2O} - \frac{p^3_{H_2} p_{CO}}{K^e_2} \right) \times \frac{1}{(DEN)^2}$$

(27)

$$r_3 = \frac{k_3}{p_{H_2}} \left(p_{CO} p_{H_2O} - \frac{p_{H_2} p_{CO_2}}{K^e_3} \right) \times \frac{1}{(DEN)^2}$$

(28)

$$r_4 = \frac{k_4}{p^{3.5}_{H_2}} \left(p_{CH_4} p^2_{H_2O} - \frac{p^4_{H_2} p_{CO_2}}{K^e_4} \right) \times \frac{1}{(DEN)^2}$$

(29)

Where DEN is defined as follows:

$$DEN = 1 + K_{CO} p_{CO} + K_{H_2} p_{H_2} + K_{CH_4} p_{CH_4} + \frac{K_{H_2O} p_{H_2O}}{p_{H_2}}$$

(30)

The value of k_i in the expressions obtained by Xu and Froment at different temperatures is obtained through the Arenus equation, $k_i = A_i . \exp(-E_i/RT)$, where A_i is the pre-exponential factor, R is the universal gas constant, and $E_{i,}$ is the activation energy for the reaction. Kinetically data for different catalysts are given in the various literature. In the modeling, modified coefficients have been used for a 5% $Ru - \gamma\, Al_2O_3$ catalyst **[17].** These coefficients are presented in Table (1).

Table 1. Kinetically parameters for 5% $Ru - \gamma\ Al_2O_3$ catalyst (activation energy in kJ/kmol) **[17]**

Reaction	**Parameters of Ru catalyst**	
1	A_1	5.6×10^{17} kmol.bar $^{-1.5}$/kg $_{cat}$.hr
	E_1	1.89×10^{5}
2	A_2	4.27×10^{15} kmol.bar $^{0.5}$/kg $_{cat}$.hr
	E_2	3.25×10^{5}
3	A_3	2.2×10^{6} kmol.bar $^{-1}$/kg $_{cat}$.hr
	E_3	5.81×10^{4}
4	A_4	7.9×10^{14} kmol.bar $^{0.5}$/kg $_{cat}$.hr
	E_4	2.69×10^{5}

Also, adsorption coefficients (K_k) change with temperature $K_k = A_k.\exp(-\Delta H_k/RT)$ so that k can be CH_4, O_2, H_2O, H_2, or CO. Adsorption coefficient constants for different materials in the reaction mechanism are presented in Table (2).

Table 2. Adsorption constants of materials for autothermal reforming process **[17]**

For r_1		**For r_2, r_3, r_4**			
$A^1_{CH_4}$	$A^1_{O_2}$	A_{CH_4}	A_{H_2O}	A_{H_2}	A_{CO}
4.02×10^{5} bar $^{-1}$	5.08×10^{4} bar $^{-1}$	6.65×10^{-4} bar $^{-1}$	1.77×10^{5} bar $^{-1}$	6.12×10^{-9} bar $^{-1}$	8.23×10^{-5} bar $^{-1}$
103.5 kJ/mol	66.2 kJ/mol	-38.28 kJ/mol	88.68 kJ/mol	-82.90 kJ/mol	-70.65 kJ/mol

The relationship between reaction equilibrium constants with temperature is as $K^e_i = K_{Oi}.\exp(-H_i/T)$ that the constants of this relationship for steam reforming equilibrium reactions are presented in Table (3).

Table 3. Equilibrium constants for the authothermal reforming process **[17]**

	K_{Oi}	H_i
$K^e_2(bar^2)$	5.75×10^{12}	26285
K^e_3	1.26×10^{-2}	-4639
$K^e_4(bar^2)$	7.24×10^{10}	21646

In this paper, the equilibrium constant for the second reaction at different temperatures was calculated with the help of thermodynamic and compared with the equilibrium constants obtained from Table (3) at the same temperatures. The relative error percentage for the equilibrium constant obtained from these two methods was less than 4%. As a result, H_i for the second reaction was considered equal to 26285 K in all simulations. The default rate equations in FLUENT software are as exponential relationships. Programming in C++ was used to consider methane autothermal reforming reactions

using a 5% $Ru - \gamma Al_2O_3$ catalyst with non-Arrhenius rate equations. This program can be used for similar rate equations.

Results

The results of CFD modeling for methane autothermal reforming on a 5% $Ru - \gamma Al_2O_3$ catalyst are presented. The considered parameters included the O_2/CH_4 ratio at the reactor inlet and inlet feed temperature.

Effect of inlet oxygen content

The reactor inlet oxygen content in this research, which is expressed as the O_2/CH_4 molar ratio, has been changed from 0.345 to 0.445, and the other operating conditions were similar to the first condition of Table (1). It is clear that the reactor inlet feed flow rate and the composition of chemical species at the reactor inlet change according to the O_2/CH_4 ratio. Figs. (3)-(6) show the concentration profile for H_2, CO, CO_2, and CH_4 along the reactor, and Fig. (7) shows the methane conversion rate versus the changes in the O_2/CH_4 ratio from 0.345 to 0.445. Fig. (8) also shows the temperature profile related to these changes.

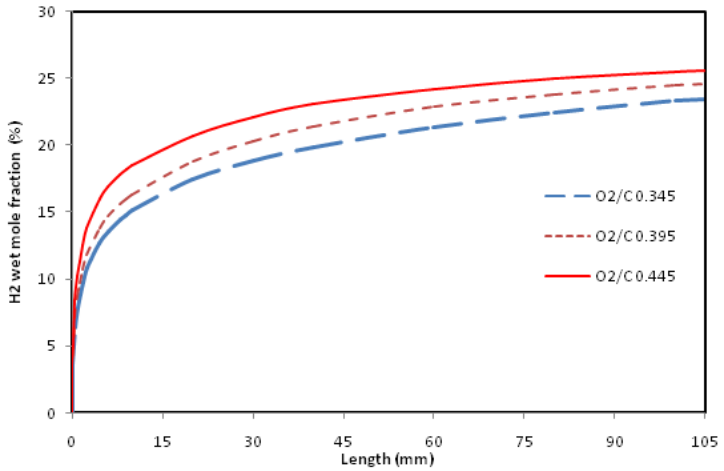

Fig. 3. A profile of hydrogen concentration vs. inlet oxygen content (H_2O/CH_4 = 2.9, thermal power 1.09 kW)

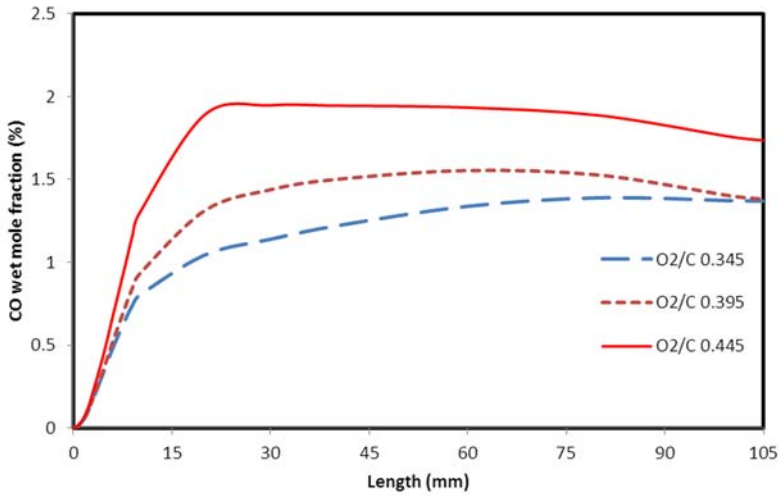

Fig. 4. A profile of carbon monoxide concentration vs. inlet oxygen content (H_2O/CH_4 = 2.9, thermal power 1.09 kW)

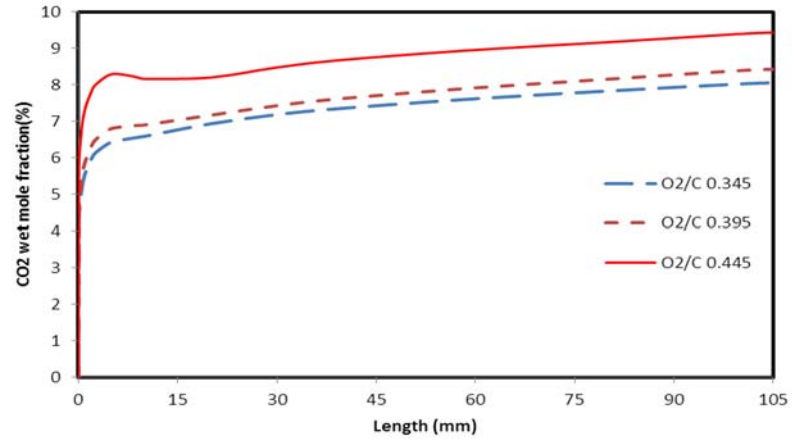

Fig. 5. A profile of carbon dioxide concentration vs. inlet oxygen content (H_2O/CH_4 = 2.9, thermal power 1.09 kW)

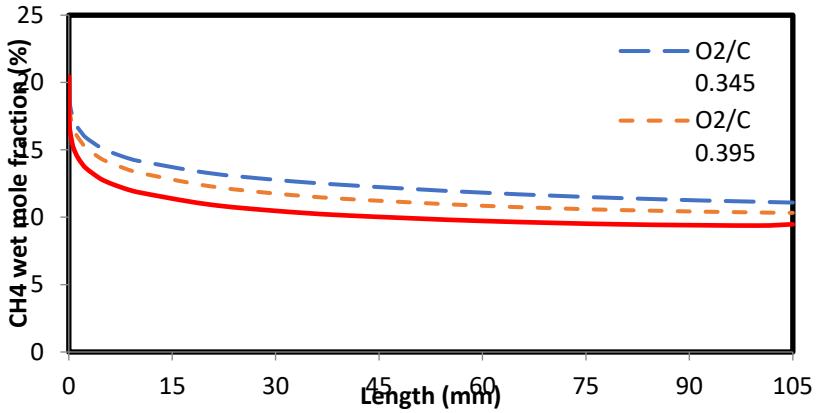

Fig. 6. A profile of methane concentration vs. inlet oxygen content (H_2O/CH_4 = 2.9, thermal power 1.09 kW)

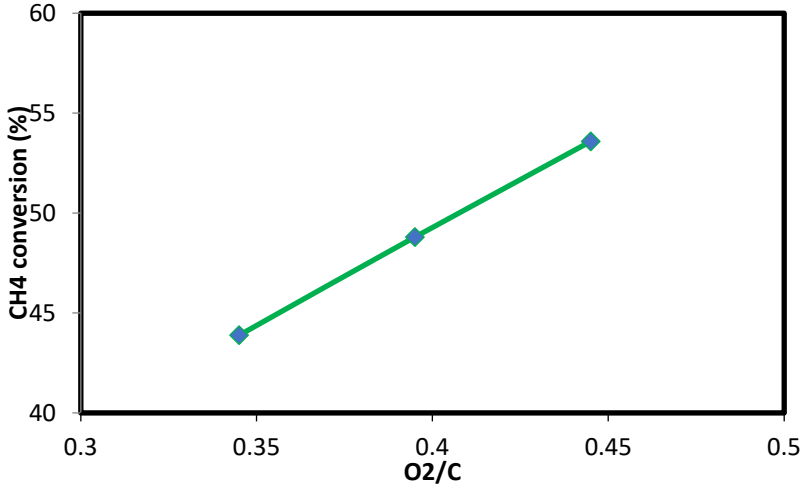

Fig. 7. The effect of inlet oxygen content on the methane conversion rate (H_2O/CH_4 = 2.9, thermal power 1.09 kW)

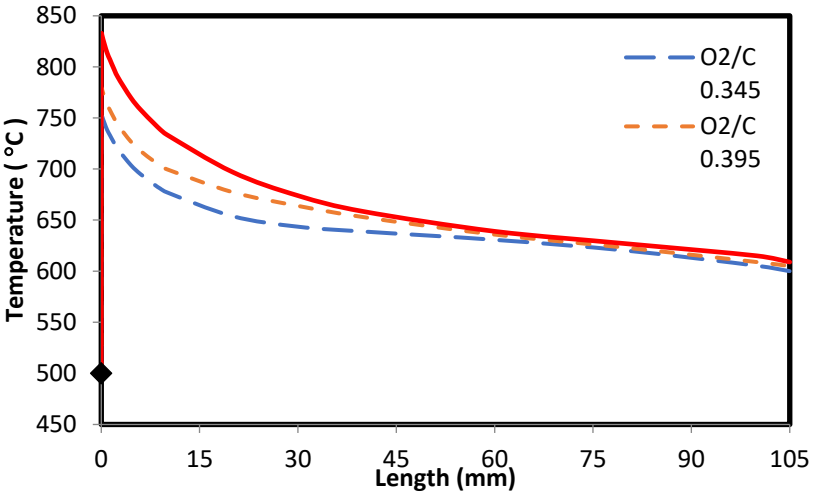

Fig. 8. A profile of temperature vs. inlet oxygen content (H_2O/CH_4 = 2.9, thermal power 1.09 kW)

As shown in Figs. (6) and (7), by increasing the reactor inlet oxygen content, more methane was consumed in the reactor and the rate of methane conversion increased. The reactor inlet methane amount was constant due to a constant inlet thermal power in these studies (1.09 kW). By increasing the reactor inlet oxygen content, more oxygen was available for the oxidation reaction, and as a result, more methane was consumed. Also, the operating temperature inside the reactor increased (Fig. 8), and the produced hydrogen content increased with the increase of reactor inlet oxygen content (Fig. 3). The above cases can be because the heat produced from the oxidation reaction is more at a higher O_2/CH_4 ratio, which can cause more progress in endothermic reforming reactions and a higher temperature gradient. Considering that hydrogen is produced in steam reforming reactions and the water-gas shift reaction (WGSR), hydrogen concentration along the reactor has an increasing behavior. The amount of produced CO also increased with the progress of reforming reactions. On the other hand, As the CO concentration increased and the temperature decreased due to steam reforming processes, the exothermic water-gas shift reaction also progressed. As a result, CO was produced in the steam reforming reaction and consumed in the water-gas shift reaction. At the end of the reactor, CO consumption exceeded its production and its concentration began to decrease. As the inlet oxygen content increased, the reforming reactions and the water-gas shift reaction occurred more intensively due to the higher reactor temperature, as a result, the amount of CO increased along the reactor and at the reactor outlet, at a higher O_2/CH_4 ratio (Fig. 4). The profile of CO_2 concentration along the reactor was also increasing due to the progress of steam reforming reactions and water-gas shift reaction. As the water-gas shift reaction progressed, the amount of CO_2 also increased while the amount of CO in the reactor decreased. At a higher O_2/CH_4 ratio, the amount of CO_2 was also higher due to the more progress in steam reforming processes and the water-gas shift reaction (Fig. 5).

Conclusions

The model presented in the present research was a 3D model for the methane autothermal reforming process, which showed the concentration and temperature changes along the monolithic catalytic bed. For this purpose, a channel of a monolithic reactor was selected as the computational domain, and the mass, energy, and momentum conservation equations were solved using FLUENT software in this computational domain. Then, the accuracy of the modeling was validated. From the comparison of the results obtained from this modeling with the laboratory work, it was founded that to achieve the maximum hydrogen content in the studied range and terms of operational parameters, the reactor inlet O_2/CH_4 and H_2O/CH_4 ratio should be selected 0.445 and 3.8, respectively.

Acknowledgments

None.

Conflict of interest

None.

Financial support

None.

Ethics statement

None.

References

1. Veser, G., Frauhammer, J. (2000). “Modelling steady state and ignition during catalytic methane oxidation in a monolith reactor”. Chemical Engineering Science, 55, 2271-2286.
2. Canu, P., Vecchi, S. (2002). “CFD simulation of reactive flows: catalytic combustion in a monolith”, AIChE Journal, 48, 2921-2935.
3. Ghadrdan M., Mehdizadeh H., (2008), “Mathematical Investigation and CFD Simulation of Monolith Reactors:

Catalytic Combustion of Methane", Excerpt from the Proceedings of the COMSOL Conference, Hannover.
4. Stutz M.J, Poulikakos D., (2005) "Effects of microreactor wall heat conduction on the reforming process of methane", Chemical Engineering Science 60, 6983 – 6997.
5. Chaniotis K., Poulikakos D. (2005), "Modeling and optimization of catalytic partial oxidation methane reforming for fuel cells", A Journal of Power Sources 142,184–193.
6. Shi. L, Bayless D. J., Prudich M., (2008), "A model of steam reforming of iso-octane: The effect of thermal boundary conditions on hydrogen production and reactor temperature", International journal of hydrogen energy, 33, 4577 – 4585.
7. Di Benedetto A., Sarli V.D, (2011), "CFD Modeling and Simulation of a Catalytic Micro-monolith", international journal of chemical reactor engineering, Volume 9, Article A21.
8. Deutschmann O. and Schmidt L.D (1998), "Two-dimensional modeling of partial oxidation of methane on rhodium in a short contact time reactor", Twenty-Seventh Symposium (International) on Combustion/The Combustion Institute, pp. 2283–2291.
9. Shi Ding, Changning Wu, Yinhong Cheng, Yong Jin, Yi Cheng (2010), "Analysis of catalytic partial oxidation of methane on rhodium-coated foam monolith using CFD with detailed chemistry", Chemical Engineering Science 65, 1989–1999.
10. Hong Mei, Chengyue Li, Shengfu Ji, Hui Liu (2007), "Modeling of a metal monolith catalytic reactor for methane steam reforming–combustion coupling", Chemical Engineering Science 62, 4294–4303.
11. Shi. L, Bayless D. J., Prudich M.,(2009), "A CFD model of autothermal reforming", International journal of hydrogen energy, 34, 7666–7675.
12. Rabe S., Truong T. B., Vogel F. (2007) "Catalytic autothermal reforming of methane: Performance of a kW scale reformer using pure oxygen as oxidant", Applied Catalysis A: General, 318, 54–62.
13. Fluent, Inc. (2006). FLUENT 6.3 User's Guide. Lebanon, NH.
14. Xu J., Froment G. (1989) "Methane Steam Reforming, Methanation, and Water-Gas Shift: I. Intrinsic Kinetics", AICHE J., Volume 35, No. 1, pp. 88-96.
15. Ma, L., Trimm, D. L., Jiang, C. (1996) "The design and testing of an autothermal reactor for the conversion of light hydrocarbons to hydrogen I. the kinetics of the catalytic oxidation of light hydrocarbons", Applied catalysis. A: General, 138, 275- 283.
16. Barrio V. L., Schaub G., Rohde M., Rabe S. (2007) "Reactor modeling to simulate catalytic partial oxidation and steam reforming of methane. Comparison of temperature profiles and strategies for hot spot minimization" International Journal of Hydrogen Energy 32, 1421–1428.
17. P. M. Biesheuvel, G. J. Kramer "Two-Section Reactor Model for Autothermal Reforming of Methane to Synthesis Gas", AIChE J. (2003), 49, 7.